



Experimental investigations on longitudinal-torsional vibration-assisted milling of Ti-6Al-4V

Philipp M. Rinck¹ · Alpcan Gueray¹ · Robin Kleinwort¹ · Michael F. Zaeh¹

Received: 3 January 2020 / Accepted: 1 May 2020 / Published online: 22 June 2020
© The Author(s) 2020

Abstract

In vibration-assisted milling (VAM), an additional high-frequency oscillation is superimposed on the kinematics of a conventional machining process. This generates oscillations of the cutting edge in the range of a few micrometers, thereby causing a high-frequency change in the cutting speed and/or the feed. Consequently, a reduction of cutting forces, an increase of the tool life, and an improvement of the workpiece quality can be achieved. This paper shows and compares the effects of longitudinal and longitudinal-torsional (L-T) vibrations on the cutting force, the tool life, and the surface quality when milling Ti-6Al-4V. In comparison with the conventional milling process, the cutting forces are significantly reduced and the surface finish of the workpiece can be improved by introducing ultrasonic vibrations to the milling process. Longitudinal-torsional vibration assistance showed better overall process performance than the pure longitudinal vibration assistance.

Keywords Vibration-assisted milling · Longitudinal-torsional vibration · Ti-6Al-4V · Cutting forces · Kinematics · Surface roughness · Burr formation

1 Introduction

The continuing trend toward lightweight construction is increasingly leading to the use of high-strength construction materials. For example, high-temperature titanium alloys are used in gas and steam turbines to increase the maximum possible temperatures in the turbine—and thus its efficiency. In medical technology, biocompatible and highly wear-resistant materials are required for the manufacture of implants and endoprostheses (e.g., teeth, hip, or knee joints)

[23]. In aerospace technology, the titanium alloy Ti-6Al-4V is used to produce structural components due to its high strength and low density [18]. For structural components of Ti-6Al-4V, the material removal by machining can be up to 95% of the total workpiece mass [8]. Considering conventional machining processes, these high-performance materials can only be machined with high cutting forces, high tool wear, and a low material removal rate. It has been proven that these problems can be successfully mitigated using vibration-assisted machining [4, 7, 24].

In vibration-assisted machining, high-frequency oscillations are added to the conventional kinematics of the machining process, thereby causing a high-frequency change in the cutting speed and/or the feed. The tool usually oscillates at a frequency over 16 kHz, with an amplitude of 1 to 20 μm . When the tool oscillates with the frequency f and a vibration amplitude A , the vibration velocity $v_{os,crit} = 2 \cdot \pi \cdot f_{os} \cdot A$ can be calculated [30]. In the case of a vibration superimposition in the cutting direction, the tool separates from the workpiece in each vibration cycle if the vibration velocity exceeds the cutting speed. This periodically interrupted process leads to several advantages compared with the conventional cutting process [25, 29]:

✉ Philipp M. Rinck
philipp.rinck@iwb.mw.tum.de

Alpcan Gueray
alpcan.gueray@tum.de

Robin Kleinwort
robin.kleinwort@iwb.mw.tum.de

Michael F. Zaeh
michael.zaeh@iwb.mw.tum.de

¹ Institute for Machine Tools and Industrial Management (iwb), Technical University Munich, Boltzmannstr. 15, 85748 Garching, Germany

- Reduced cutting forces
- Increased machining stability
- Reduced tool wear
- Improved workpiece quality

Figure 1 shows different types of vibration-assisted machining, which can be distinguished by the characteristics of the tooltip trajectory. In 1D vibration-assisted machining, the cutting tool vibrates either in the cutting direction or in direction perpendicular thereto. If the tooltip vibrates simultaneously in both the cutting and normal direction at different frequencies or with a phase difference, the tooltip will perform an elliptical motion [19]. This process is called 2D vibration-assisted machining. In vibration-assisted turning, the influence of the tooltip trajectory on the process performance has already been studied extensively [10, 20, 30]. Most of the publications state that a vibration superimposition in cutting direction yields more benefits regarding a reduction in cutting forces and tool wear than a superimposition perpendicular to the workpiece surface [30].

Vibration-assisted machining has already been studied for over 50 years [2]. It has been applied to machining processes like turning, drilling, milling, and grinding. The vibration assistance can be achieved by either vibrating the tool or the workpiece. Most of the researches were focused on vibration assisted turning (VAT), as it is easier to apply ultrasonic vibrations to a stationary turning tool rather than to a rotating, drilling, milling, or grinding tool.

Nath et al. [11] studied the effects of vibration-assisted turning of Inconel 718 with vibrations in the cutting direction regarding cutting forces, tool wear, surface quality, and chip formation. During the experiments, the cutting speed and the feed rate were varied and the ultrasonic vibration frequency and the amplitude were kept constant at 19 kHz and 15 μm respectively. The results showed that the surface quality depends mostly on the tool-to-workpiece contact ratio and the relative speed between the tool and

the workpiece when machining with vibration assistance. It was found that to achieve high cutting qualities, the tool-workpiece contact ratio must be kept low, which can be achieved by increasing the amplitude and the frequency of the vibration or decreasing the cutting speed. The resulting cutting forces during vibration-assisted turning were reduced by 75 to 88% compared with conventional turning. The tool life of the cubic boron nitride cutters used was increased 4 to 8 times during turning with vibration assistance with a cutting speed of 10 m/min. However, beyond 10 m/min cutting speed, tools catastrophically failed under ultrasonic vibration assistance. Ultrasonic vibration assistance enabled surface finishes of $R_a \leq 1 \mu\text{m}$, whereas the best surface roughness achieved with conventional turning was $R_a = 2.4 \mu\text{m}$. It was mentioned that vibration assistance caused longer, thinner chips, which is favorable for high-quality machining. Patil et al. [16] studied the effects of feed direction ultrasonic vibration assistance during dry turning of Ti-6Al-4V. The cutting speed and the feed rate were varied and the ultrasonic vibration frequency and the amplitude were kept constant at 20 kHz and 20 μm, respectively. A cutting force reduction of up to 50% was observed due to the vibration assistance, and an increasing tool-workpiece contact ratio resulted in a decrease in force reduction. Better surface quality and thinner, longer chips were observed with vibration assistance. Another important effect of vibration-assisted machining is the influence on the residual stress state near the surface of the machined workpiece. Nestler et al. [12] showed that higher compressive residual stresses can be achieved by applying the vibration assistance perpendicular to the machined surface. Similar results are shown in [29] regarding residual stresses. For vibration-assisted turning of Ti-6Al-4V, several approaches for numerical modelling of the cutting mechanism exist [16, 22]. Cakir et al. [3] modelled the chip formation mechanism and showed that the average cutting force significantly drops with vibration assistance due to the intermittent cutting effect, which in turn may improve the tool life. Although the cutting edge has the possibility to cool down when the tool separates from the workpiece, the peak temperature during each vibration cycle was found to be higher compared with conventional turning.

Compared with VAT, VAM has not yet been thoroughly investigated. In VAM, two different methods for superimposing an ultrasonic vibration exist. The first one involves using an ultrasonic worktable, which excites the workpiece with the ultrasonic vibration [1]. Although the installation of an ultrasonic worktable is relatively easy, this method has some disadvantages. When different workpieces are milled, the ultrasonic system needs to be adjusted because of a change of the systems' resonance frequency. A more flexible method is achieved by superimposing the vibration on

Type	Vibration in cutting direction	Vibration normal to the surface	Vibration normal to cutting direction	Combined vibration
Trajectory				
Displacement	$x(t) = v_c t + A_x \cos(2\pi f t)$ $y(t) = 0$ $z(t) = 0$	$x(t) = v_c t$ $y(t) = A_y \sin(2\pi f t)$ $z(t) = 0$	$x(t) = v_c t$ $y(t) = 0$ $z(t) = A_z \sin(2\pi f t)$	$x(t) = v_c t + A_x \cos(2\pi f t)$ $y(t) = A_y \sin(2\pi f t + \phi_1)$ $z(t) = A_z \sin(2\pi f t + \phi_2)$

Fig. 1 Types of vibration-assisted milling

the milling tool. Usually, the tool is superimposed with a longitudinal vibration along its axis (longitudinal vibration-assisted milling (LVAM)). Many researchers reported positive effects regarding surface roughness, cutting forces, and tool life [9, 13, 24, 25, 27, 31]. Razfar et al. [17] studied the effects of longitudinal vibration-assisted milling of AISI 1020 steel by superimposing a vibration on the workpiece. Experiments were carried out at a constant vibration frequency of 20 kHz. During the experiments, the depth of cut, the cutting speed, and the feed rate were varied. While the positive effect of vibration superimposition tended to decrease with increasing cutting speed and feed rates, an increase in depth of cut did not result in a significant deterioration of the surface quality. A decrease in the cutting force was observed during the intermittent cutting process, which was explained both by an aerodynamic lubrication effect and by the improved cooling behavior of the tool. A positive correlation between the tool-workpiece separation time and the reduction in cutting forces was found. Niu et al. [15] studied longitudinal-torsional vibration-assisted milling (LTVAM) of Ti-6Al-4V by superimposing the vibrations on the milling tool. The torsional vibrations were produced by degenerating longitudinal vibrations into torsional vibrations by helical grooves in the sonotrode. The research included the influence of the ultrasonic vibration on residual stresses, surface hardness, and surface quality of the milled workpiece. The ultrasonic vibration frequency was kept constant at 35 kHz and the amplitude was varied between 2 and 6 μm . The experiments showed that the vibration amplitude has the least significant effect on residual stresses. However, sensitivity analysis revealed that a higher vibration amplitude increases the surface hardness of the bottom surface, which is explained by the increase of the impact energy with the increasing vibration amplitude. Zhou et al. [33] studied the cutting mechanisms in the hole-making process of longitudinal-torsional ultrasonic-assisted helical milling. The results showed a reduction in the axial cutting force of up to 12%, whereas the other cutting force components did not change significantly compared with conventional helical milling. An overall reduction in the burr height at the hole entry was also achieved. Similar experiments were performed by Wu et al. [28], who studied a longitudinal-torsional vibration-assisted side milling process. The measured reduction in the cutting forces was 45.8% in the x -direction, 27.6% in the y -direction, and 48% in the z -direction. Wu et al. also stated that the cutting force reduction is in correlation with the total contact time between the tool and the workpiece. With a higher contact time, a decrease of the force reduction was observed. Thus, a higher cutting speed also resulted in a lower force reduction.

In the present work, the influence of LVAM and LTVAM on machining Ti-6Al-4V is demonstrated and compared with each other for the first time. After analyzing the

process kinematics of LVAM and LTVAM in chapter 4, an ultrasonic actuator is presented that is capable of superimposing longitudinal and longitudinal-torsional vibrations onto an endmill. Experiments were carried out for slot and peripheral milling. In Section 4.1, the effects of LVAM and LTVAM on the cutting forces are discussed. The resulting workpiece properties in the form of surface roughness, residual stresses, hardness, and burr formation are described in Section 4.2. The effect on the tool life is shown in Section 4.3.

2 Kinematic analysis of LTVAM with helical end mills

In vibration-assisted milling, the conventional kinematic of the cutting tool is superimposed by an additional vibration. The resulting process kinematics of a L-T vibration will be discussed in the following. The movement of the cutting tool in conventional milling consists of the cutting motion and the feed motion. The two-dimensional trajectory of a point at the cutting edge is shown in Fig. 2 (top), where the current position of the point is a function of time t , spindle speed n , tool diameter D , and the feed rate v_f . Due to the longitudinal vibration assistance, each point of the tool vibrates along the z -axis. This superimposed vibration movement is a function of time t , vibration frequency f_{os} , and vibration amplitude A_l . The longitudinal vibration assistance causes a high-frequency, reciprocating movement along the tool's axis. In Fig. 2 (middle), the trajectory of a cutting edge for one tool rotation under the influence of a longitudinal vibration is shown. Torsional vibration assistance causes a reciprocating movement that acts in the x - and the y -directions. The reciprocating motion of a point on the cutting edge caused by the L-T vibration can be calculated using the following equation where A_t is the

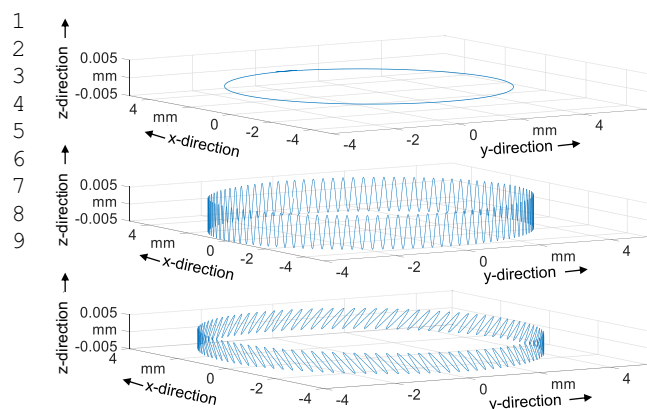


Fig. 2 Schematic trajectory of the cutting edge for one tool rotation. Conventional milling (top), LVAM (middle) and LTVAM (bottom)

torsional vibration amplitude:

$$\begin{aligned} x(t) &= \frac{d}{2} \cdot n(2 \cdot \pi \cdot n \cdot t + A_t \cdot n(2 \cdot \pi \cdot f_{os} \cdot t)) + v_f \cdot t \\ y(t) &= \frac{d}{2} \cdot \cos(2 \cdot \pi \cdot n \cdot t + A_t \cdot n(2 \cdot \pi \cdot f_{os} \cdot t)) \\ z(t) &= A_l \cdot n(2 \cdot \pi \cdot f_{os} \cdot t + \phi) \end{aligned} \tag{1}$$

In order to determine whether the cutting tool loses contact with the workpiece due to the vibration assistance, the vibration velocity in the cutting direction can be calculated for LVAM and LTVAM by

$$v_{os,crit} = 2 \cdot \pi \cdot f_{os} \cdot A_t + 2 \cdot \pi \cdot f_{os} \cdot A_l \cdot \tan(\beta) \tag{2}$$

where β is the helix angle of the milling tool. When the vibration velocity $v_{os,crit}$ exceeds the cutting speed v_c , the cutting edges will lose contact with the workpiece in each vibration cycle, resulting in an intermittent cutting process. If the vibration velocity $v_{os,crit}$ does not exceed the cutting speed v_c , the tool will not lose contact with the workpiece, resulting in a continuous cutting process with an ultrasonically modulated cutting speed. The principle of the intermittent cutting process can be seen in Fig. 3. The figure shows the position of a point on the cutting edge in cutting direction for conventional machining (p_{con}) and for vibration-assisted machining (p_{os}), which can be derived from Eq. 2.

When the cutting edge moves opposite to the direction of cutting, the rake face of the tool loses contact with the chip (exit point t_e). From that point on, the cutting forces drop significantly. It should be noted that although the cutting process stopped, the flank face of the tool is still in contact with the workpiece, creating frictional forces. Between the points t_e and t_t (turning point), the friction force acts opposite to the cutting direction. When the cutting edge passes the turning point t_t , the friction force acts in the cutting direction. The cutting process starts again when the cutting edge reaches the start point (t_s). The result is an intermittent cutting process, which is repeated periodically

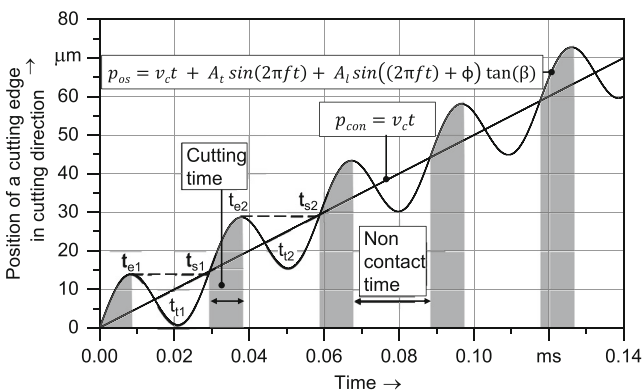


Fig. 3 Position of a point on the cutting edge in cutting direction under the influence of a longitudinal-torsional vibration

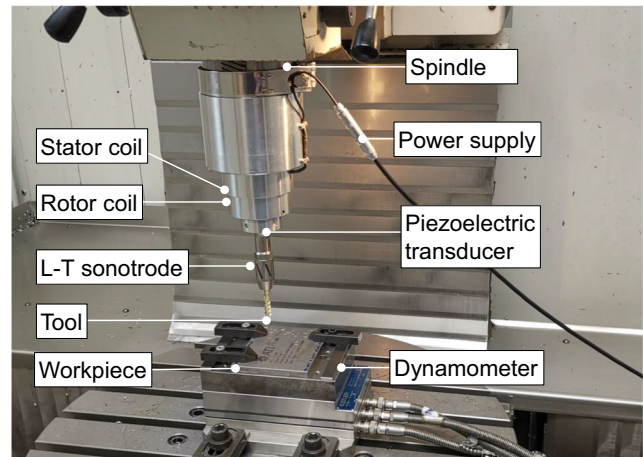


Fig. 4 Experimental setup for peripheral milling and slot milling with longitudinal-torsional vibration assistance

with each vibration cycle. The ratio of relative cutting time T_c can be calculated by:

$$T_c = \frac{t_{e2} - t_{s1}}{t_{s2} - t_{s1}} \tag{3}$$

Many researchers already stated that the relative cutting time is directly proportional to the cutting force in vibration-assisted machining. In order to achieve a lower cutting time T_c , the vibration amplitude and the frequency must be increased or the cutting speed must be decreased.

3 Experiments

3.1 Experimental setup

The experiments were carried out on a CNC milling machine (Hermle UWF 900), as seen in Fig. 4. The cutting forces were measured in x -, y -, and z -directions with a dynamometer (Kistler 9257A). To determine the surface roughness in accordance with DIN EN ISO 4287, a 3D laser scanning microscope (Keyence VK-X1000) was used. The residual stresses were analyzed with an X-ray diffractometer (Stresstech XSTRESS G2R with Ti-X-ray tube). Hardness measurements were carried out with a Vickers hardness tester (LECO LV-Series). The workpiece made from Ti-6Al-4V had the dimensions $100 \times 100 \times 5$ mm. The chemical properties of the titanium alloy are shown in Table 1.

The solid carbide milling tool with 3 flutes has a diameter of 8 mm, a helix angle of 55° , a positive rake angle,

Table 1 Chemical composition of the workpiece material

% Al	% V	% Fe	% O ₂	% N ₂	% H ₂	% Ti
6.18	3.96	0.18	0.15	< 0.01	< 0.001	rest

Table 2 Overview of the parameter range that was used for full factorial DoE; for peripheral milling, the experiments were performed with a constant axial depth of cut a_p of 5 mm and a radial depth of cut a_e of 0.5 mm

Level	Cutting speed v_c in m/min	Feed per tooth f_z in mm	Amplitude A_l in μm	Frequency f in Hz
1	30	0.04	0	0
2	80	0.05	≈ 4	$\approx 32,000$
3			≈ 6	
4			≈ 8	
5			≈ 10	
6			≈ 12	

Slot milling was performed with a depth of cut a_p of 0,5 mm. Each experiment was carried out twice

and a free angle $> 9^\circ$. The tool is PVD coated with ZrN (zirconium nitride) because of its low chemical affinity to Ti-6Al-4V, which reduces adhesive tool wear during milling.

The parameter range used for the experiments is given in Table 2.

3.2 Ultrasonic actuator

To superimpose an ultrasonic vibration onto the milling tool, an ultrasonic actuator was designed in ANSYS. The actuator consists of a Langevin–Bolt transducer that converts a high-frequency electrical current into a mechanical vibration. The

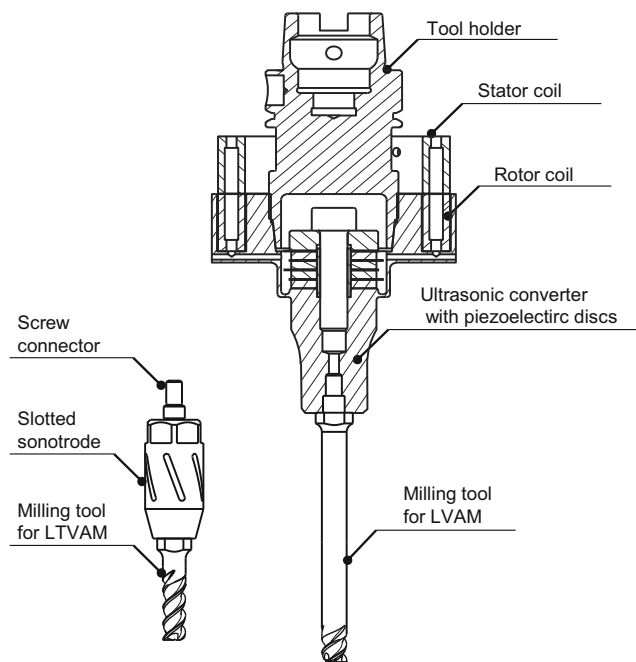


Fig. 5 Actuator for ultrasonically assisted milling with the milling tool for LVAM and sonotrode with the milling tool for LTVAM

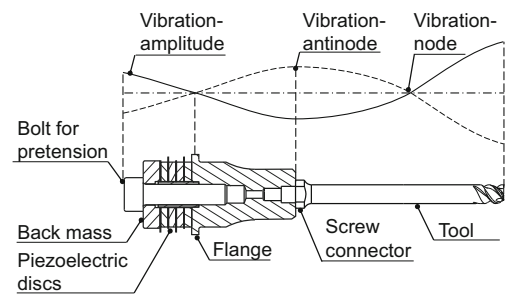


Fig. 6 Ultrasonic converter with milling tool; the vibration amplitude is schematically shown along the actuator with its amplitude maximum at the tooltip

transducer is powered by an ultrasonic generator (Weber Typ ULC MD/MFD). The electrical energy is transferred via induction through a stator and rotor coil to the rotating transducer. In order to generate a pure longitudinal vibration at the tool center point, a customized milling tool that resonates at its first longitudinal eigenmode at 34 kHz was designed and fabricated. The milling tool is attached to the transducer using a screw connection with an axial centering. This method ensures minimal damping of the vibration amplitude when compared with conventional collet chucks. The length of the cutting edges was kept short to prevent the longitudinal vibration mode from being converted into a torsional vibration mode through the helix form of the cutting edges.

In order to generate a longitudinal-torsional vibration output at the tool center point, a slitted horn was designed. By means of geometrical changes of the cross section of the horn, a part of the longitudinal vibration is converted into a torsional vibration. The helical form of the cutting

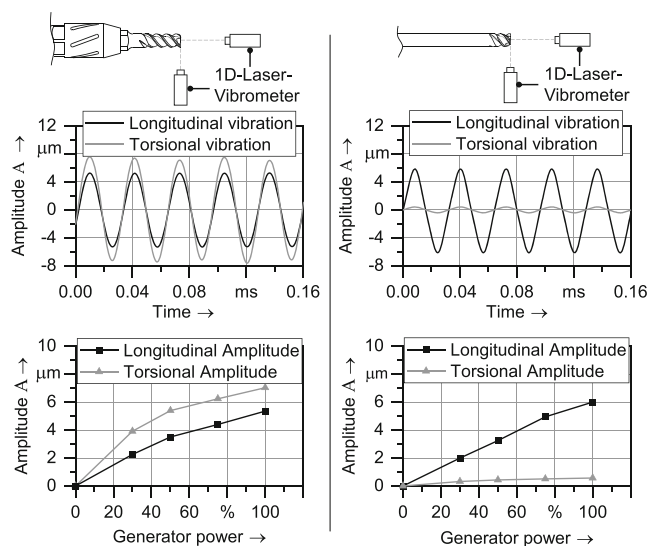


Fig. 7 Longitudinal and torsional vibration amplitude (peak to peak) at the cutting edges in LTVAM (left) and LVAM (right); the amplitude can be adjusted by changing the generator power output

edges further amplifies the torsional vibration output. The actuator is shown in Fig. 5, and the converter in Fig. 6, and the longitudinal and torsional vibration output on the cutting edge is depicted in Fig. 7. The achieved ratio between torsional and longitudinal vibration outputs in LTVAM (A_t/A_l) is about 1.3. In the following descriptions, only the longitudinal vibration amplitude A_l will be given. For LTVAM, the corresponding torsional amplitude can be calculated by:

$$A_t = 1.35 \cdot A_l \tag{4}$$

The amplitude at the cutting edges can be adjusted to a certain extent (A_l between approximately 4 and 12 μm) by adjusting the output power of the ultrasonic generator.

4 Results and discussion

In the following, the effects of ultrasonic vibration assistance on the milling forces, workpiece properties, and tool wear will be discussed.

4.1 Effect on the cutting force

Figure 8 shows the cutting force in relation to the longitudinal vibration amplitude A_l for LVAM and LTVAM for different cutting speeds for peripheral milling. Ultrasonic assistance reduces the cutting forces significantly due to the intermittent cutting process and the reduced macroscopic friction coefficient between the tool and the workpiece. The highest cutting force reduction for LVAM in comparison with conventional milling ($A_l = 0$) is 44% for F_x , 47% for F_y , and 44% for F_z at a vibration amplitude A_l of 11.8 μm . In LTVAM, the highest force reduction is 53% for F_x , 59% for F_y , and 61% for F_z at a vibration amplitude A_l of 11.8 μm . The gray parts in Fig. 8 indicate the regions in which the cutting tool was in constant contact with the workpiece according to Eq. 2. For a cutting speed of $v_c = 30$ m/min, the tool loses contact with the workpiece at a vibration amplitude of $A_l = 4.6$ μm for LVAM, whereas in LTVAM, only a longitudinal vibration amplitude of 1.7 μm is needed. For a cutting speed of $v_c = 80$ m/min, no tool-workpiece separation occurs for LVAM. In the region, where $v_{os,crit} < v_c$, the reduction in cutting forces is moderate. Here, the force reduction can be explained by an ultrasonic modulation of the cutting speed, which decreases the macroscopic friction coefficient between the rake face and the flowing chip, and between the flank face and the workpiece, thus creating a higher shear angle when compared with conventional machining. When the vibration amplitude is increased until the vibration velocity $v_{os,crit}$ equals the cutting speed v_c , the cutting edge loses contact. In this

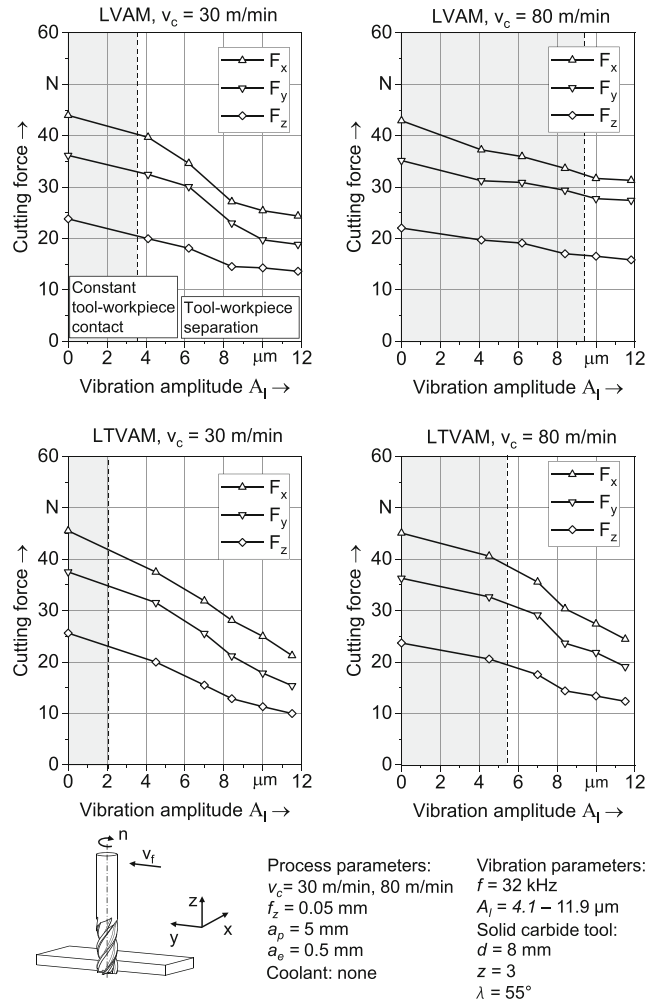


Fig. 8 Cutting forces F_x , F_y , and F_z for peripheral milling at different vibration amplitudes for $v_c = 30$ m/min (left) and $v_c = 80$ m/min (right). Top: LVAM. Bottom: LTVAM

region, as described in Section 4, the friction force temporarily acts opposite to the cutting direction which lowers the average cutting forces considerably. LTVAM shows a higher reduction than LVAM because the torsional component of the vibration leads to a lower contact time. The effects described are equal for LVAM and LTVAM, whereas LTVAM shows lower cutting forces in all regions.

4.2 Effect on surface roughness, residual stresses, and burr formation

The effects of vibration-assisted milling on the workpiece properties are discussed in the following. The results are described for the side wall of the workpiece for peripheral milling and for the bottom surface for slot milling.

Surface roughness of the bottom surface Figure 9 (top) shows the resulting average roughness value R_a for different vibration amplitudes. At a vibration amplitude of

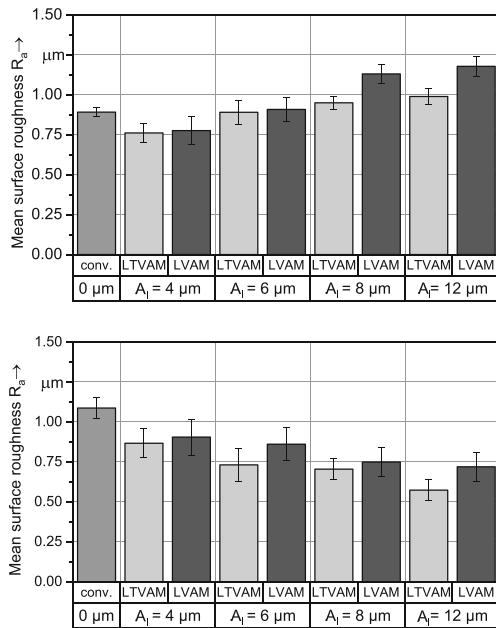


Fig. 9 Resulting surface roughness for slot milling (top) and peripheral milling (bottom) with different vibration amplitudes for LVAM and LTVAM

$A_l = 4 \mu\text{m}$, the surface roughness decreased for both LVAM and LTVAM from $R_a = 0.9$ to $0.78 \mu\text{m}$ and $0.75 \mu\text{m}$, respectively. Microscopic images (Fig. 10) show that the feed marks are reduced compared with conventional milling, which reduces the corresponding surface roughness. When the vibration amplitude is increased further, the surface roughness also increases slightly for both LVAM and LTVAM. The surface shows vibration marks that increase with rising vibration amplitude. In all cases, LTVAM shows a better surface roughness when compared with LVAM.

Surface roughness of the side wall Different results occur when the surface roughness of the side wall for peripheral milling is analyzed. With increasing amplitude, the surface

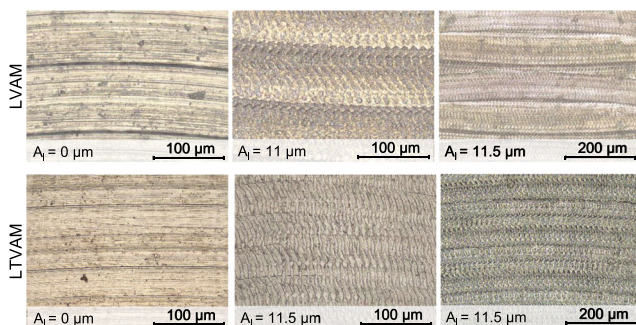


Fig. 10 Images of the bottom surface for slot milling for LVAM and LTVAM at a cutting speed of $v_c = 30 \text{ m/min}$ with different magnifications

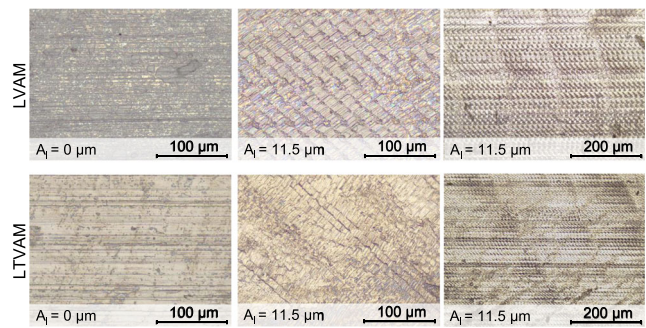


Fig. 11 Images of the side wall surface for peripheral milling for LVAM and LTVAM at a cutting speed of $v_c = 30 \text{ m/min}$ with different magnifications

roughness is reduced for LVAM and LTVAM, whereas the latter shows lower values overall. Images of the resulting surfaces are shown in Fig. 11. The effect of the ultrasonic vibration smoothens the surface as micropeaks are flattened by the oscillating cutting edge. Other researchers stated that the resulting surface has beneficial properties such as a higher oil-locking property, which can improve the friction coefficient [21, 25].

Residual stresses and surface hardness The machining of Ti-6Al-4V inevitably leads to changes in the near-surface residual stresses, due to the high mechanical and thermal loads between the tool and the workpiece during the milling process [5]. The thermal load usually causes tensile stresses near the surface. The friction between the tool and the workpiece (especially the friction between the flank face and the workpiece) causes the surface layer to heat up locally and expand, which initially induces compressive stresses. If the yield point of the material is exceeded by these loads, plastic compression occurs. When the previously compressed region cools down and stretches, tensile residual stresses occur. The mechanical load usually generates compressive residual stresses in the

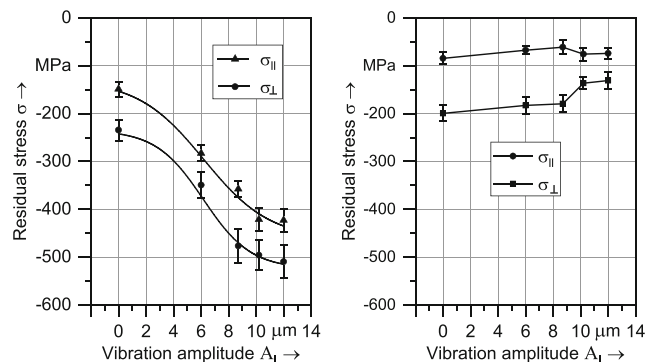


Fig. 12 Residual stresses in feed direction and normal to feed direction for different vibration amplitudes in LVAM; left: bottom surface for slot milling; right: side surface for peripheral milling

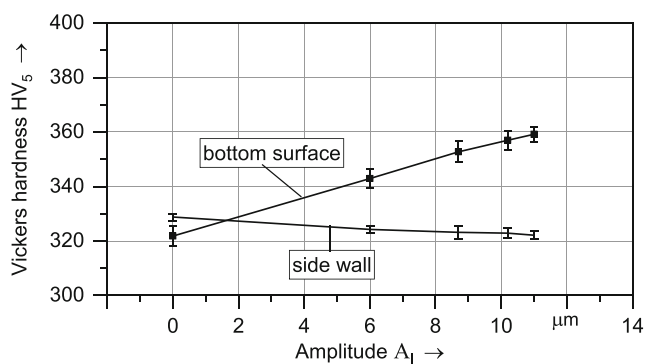


Fig. 13 Vickers hardness at the bottom surface and at the side wall for LVAM

cutting direction by preventing elastic deformation through areas where plastic deformation has already occurred. The residual stress state influences the workpiece properties regarding fatigue life and corrosion resistance. Compressive stresses are to be preferred since tensile stresses applied must first exceed the level of the residual compressive stresses before the material would be loaded at all [29].

The influence of the vibration amplitude in LVAM and LTVAM on the surface residual stresses in the feed, as well as in its corresponding normal direction, is shown in Fig. 12 for peripheral and slot milling. In slot milling (Fig. 12 left), the compressive residual stresses on the surface rise with higher amplitudes for both LVAM and LTVAM. The longitudinal vibration component causes repeated impacts between the tool and the bottom surface. These impacts have an effect similar to shot peening, thus creating higher compressive residual stresses. LVAM shows a rise in compressive stresses in feed direction from 240 MPa for conventional milling to 508 MPa with an amplitude A_l of 12 μm . In LTVAM, on the other hand, the compressive stresses in feed direction increase from 240 to 465 MPa at a vibration amplitude A_l of 11.4 μm . The lower compressive stresses in LTVAM may be explained by the reduced contact time between the tool and the workpiece due to the torsional vibration component and its correspondingly higher reduction of cutting forces. The reduced contact time in vibration-assisted milling also results in a lower temperature in the process zone, as has already been described by [26]. Figure 14 shows temperatures measured with thermoelements that were embedded in the workpiece for LVAM and LTVAM. The thermoelements were placed in drilled holes at a distance of 0.1 mm from the milled surface. Although the measured temperatures do not represent the temperatures in the cutting zone (as these are much higher), it is possible to conclude that the heat transfer into the workpiece is lower for both LVAM and LTVAM than for conventional milling. LTVAM shows a greater drop in temperature, mainly due to a lower tool–workpiece contact

time and reduced friction. The lower heat transfer into the workpiece and the corresponding lower temperatures also contribute to higher compressive residual stresses because high temperatures lead to tensile residual stresses. In peripheral milling, the effect of the ultrasonic vibration on the residual stresses of the side wall showed a different effect than in slot milling. The resulting residual stresses for different vibration amplitudes are depicted in Fig. 12 (right) for LVAM. With higher amplitudes, the residual stresses tend to become less compressive. This can be explained by reduced cutting forces, and thus lower mechanical loads on the surface. In comparison with slot milling, in peripheral milling, there is no impact mechanism through the vibration that causes higher compressive residual stresses.

The surface hardness correlates with the measured residual stresses. Figure 13 provides the Vickers hardness for LVAM for the side wall and the bottom surface. On the bottom surface, the hardness increases from HV 322 to HV 359 with rising amplitude because of the hardening effect of the tool–workpiece impacts. On the side wall, the hardness decreases from HV 328 to HV 322 with rising amplitude. The lower cutting forces with rising amplitude lead to a lower hardness (Fig. 14).

Burr formation A burr is a part of the material that remains attached to the edge of a workpiece after the machining process [6]. As the deburring process of machined parts is time consuming and expensive, burr formation should be minimized [32]. In this study, the burr height at the down-milling side is analyzed. The burr height was measured at 5 different defined points at the edge of a workpiece and the average burr height was calculated. Figure 15 presents the result in relation to different cutting speeds as well as

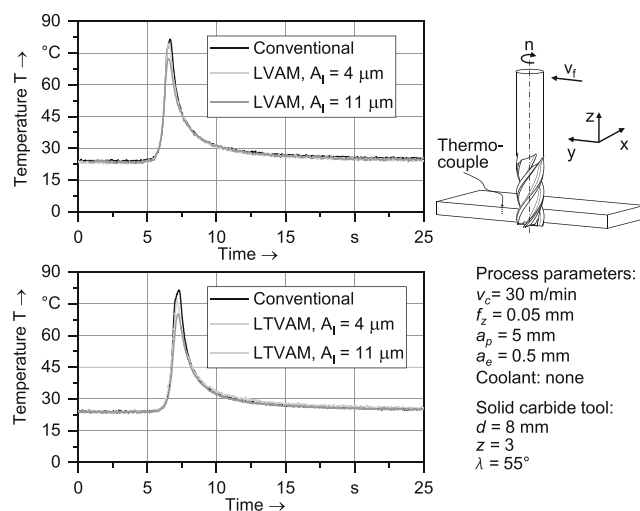


Fig. 14 Temperature measurement for LVAM (top) and LTVAM (bottom) with a thermocouple embedded in the workpiece for peripheral milling at different vibration amplitudes

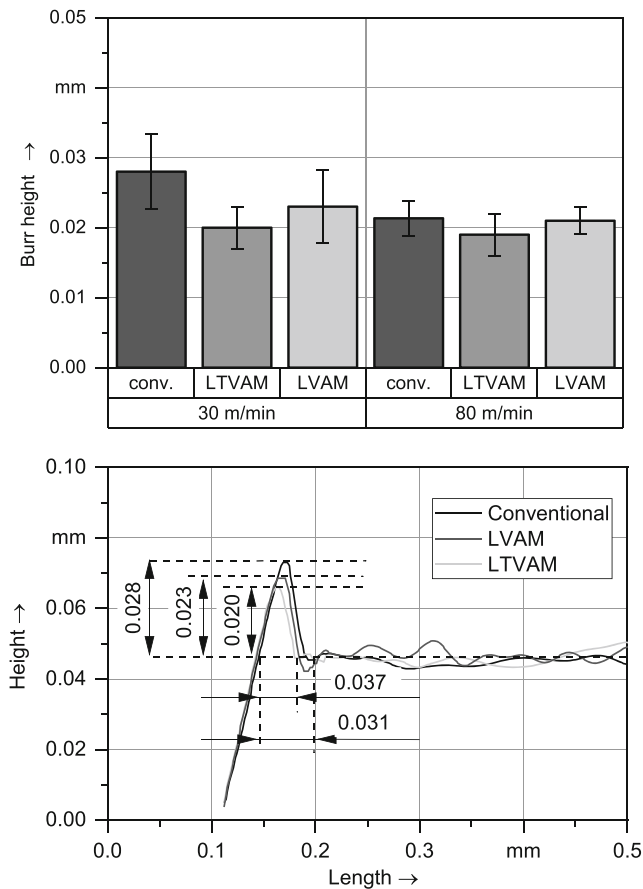


Fig. 15 Top burr height at the down-milling side for different cutting speeds and exemplary measurements of the burr height with $v_c = 30$ m/min, $f_z = 0.05$ mm, $a_p = 5$ mm, $a_e = 0.5$ mm, and $A_l = 11.9 \mu\text{m}$

sample measurements of the burr height at given process parameters. Both LVAM and LTVAM show very similar results in comparison with conventional milling. A slight reduction from 0.029 to 0.020 mm (LTVAM) and 0.023 mm (LVAM) can be noticed at a cutting speed of $v_c = 30$ m/min. At higher cutting speeds, no significant differences in burr height between vibration-assisted milling and conventional milling were observed. The mechanisms of burr formation in milling are very complex and are not yet fully understood [14], but it has already been stated that the top burr height increases with a higher friction coefficient. Thus, vibration-assisted machining can reduce burr formation as it reduces the friction between the tool and the workpiece.

4.3 Effect on tool wear

Due to the poor thermal conductivity of titanium, a considerable amount of the heat generated during machining is dissipated via the tool, which leads to high thermal loads on the cutting edge and promotes chemical reactions between the workpiece and the cutting edge. In addition, the low

modulus of elasticity combined with high tensile strength causes a high load on the cutting edges, resulting in high tool wear. As shown in Fig. 16, vibration-assisted machining has a significant influence on the tool wear.

For peripheral milling (Fig. 16 top), the primary cutting edge was analyzed in regard to abrasive flank wear, adhesion wear, and chipping. Both LVAM and LTVAM showed less tool wear compared with conventional dry milling. With LTVAM, the milling distance was increased from 12 to 15 m (+ 20%) until a wear mark of 0.20 mm was reached. LVAM increased the tool life to 14.5 m traverse in feed direction (+ 17.2%). The predominant tool wear mechanism was abrasive flank wear. Occasionally, chipping was observed along the cutting edge. Abrasion wear mostly occurs due to the friction between the tool and the workpiece. Because of the lower cutting forces and temperatures, as well as the lower friction between the tool and the workpiece in vibration-assisted milling, abrasive wear is reduced. LTVAM demonstrates better performance than LVAM because of even lower forces and temperatures. Furthermore, adhesive wear in the form of built-up edge was reduced in LTVAM and LVAM. Adhesive wear occurs when a part of the workpiece material adheres to the tool because of high pressures, high temperatures, and a high chemical affinity between the tool and the workpiece. The lower temperatures and cutting forces and the reduced

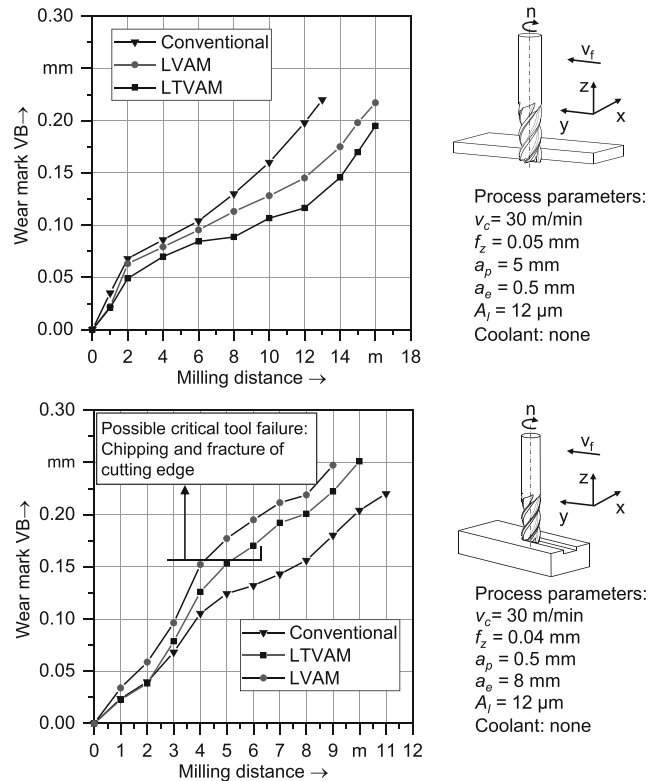


Fig. 16 Tool wear for conventional milling, LVAM, and LTVAM on the primary (top) and minor (bottom) cutting edges

friction in vibration-assisted milling significantly reduced the occurrence of built-up edges, whereas conventional milling showed small amounts of built-up layers. Another factor that could have caused the reduced tool wear in VAM is the lower contact time between the tool and the workpiece, as diffusion mechanisms are suppressed if there is no contact. For slot milling, different wear mechanisms were observed (Fig. 16 bottom). In comparison with conventional milling, both LVAM and LTVAM showed higher flank wear. The tool life decreased in LTVAM from 11 to 9 m traverse (− 18.2%) and in LVAM to 8 m (− 33.3%) until a wear mark of 0.20 mm was reached. The predominant factor in increasing the flank wear seems to be the longitudinal part of the vibration, which creates a ploughing force on the flank face of the milling tool. LTVAM shows slightly less tool wear which is because of the lower friction and temperature in comparison with LVAM. At cutting lengths above 4 m, occasional chipping on the tool nose was observed in LVAM and LTVAM. Chipping occurs due to high mechanical stresses and high temperatures at the cutting edge. These stresses lead to microscale cracks, which will eventually cause chipping through crack propagation. Although the temperature is lower in LVAM and LTVAM than that in

conventional milling, the probability of chipping is higher. This may be due to the mechanical loads that are caused by the longitudinal vibration component. The longitudinal vibration causes high-frequency impacts between the minor cutting edge and the workpiece that enhance the formation and propagation of microcracks, which eventually will lead to chipping of the outer cutting edge (Fig. 17).

5 Conclusion and outlook

This paper presents an approach to enhance the machining performance during milling of materials that are difficult to cut, such as Ti-6Al-4V. An ultrasonic actuator for superimposing longitudinal and longitudinal-torsional vibrations on an end mill is shown. The resulting kinematics of the milling tool is described. Experimental results for peripheral milling and slot milling allow the following conclusions:

- Cutting forces decrease significantly in vibration-assisted milling of Ti-6Al-4V. In LVAM, an average maximum decrease in the cutting force of 44.3% can be observed for peripheral milling. A positive correlation between the cutting forces and the contact time between the tool and the workpiece was observed. A higher contact time leads to less force reduction. LTVAM leads to a further decrease in cutting forces (57%), as the torsional-vibration component leads to a lower contact ratio.
- The bottom surface roughness of the slot-milled specimens decreases from $R_a = 0.9$ to $0.78 \mu\text{m}$ (LVAM) and $0.75 \mu\text{m}$ (LTVAM) with a vibration amplitude A_l of $4 \mu\text{m}$. With a further increase in vibration amplitude, the surface roughness of the side wall improves for both LVAM and LTVAM with increasing vibration amplitude.
- LVAM and LTVAM can significantly increase the compressive residual stresses and the surface hardness in slot milling. For peripheral milling, the ultrasonic vibration only has a small influence on residual stresses.
- Burr formation can be slightly reduced by vibration assistance.
- Vibration assistance increases the tool wear of the minor cutting edges, whereas the tool wear of the primary cutting edges is reduced by up to 20%. LTVAM consistently shows lower tool wear than LVAM.

The reductions in cutting forces in LVAM and LTVAM, even in the region without an interruption of the cutting process, need further investigation and modeling in order to get a better understanding of the friction forces between the tool and the workpiece and its influence on the chip formation. In the region of an interrupted cutting process, different cutting fluids and coolants have a significant potential to further

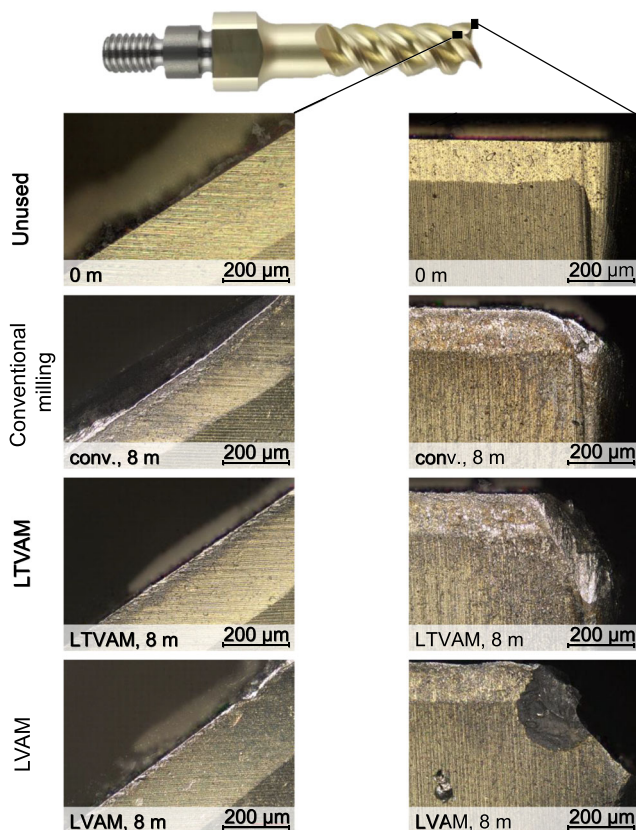


Fig. 17 Images of the tool wear for conventional milling, LVAM, and LTVAM on the primary (left) and minor (right) cutting edges

improve process performance, as the vibration may make the cutting zone more accessible for the coolant. Future research will investigate the influence of cryogenic cooling or minimum quantity lubrication on the process.

Funding information Open Access funding provided by Projekt DEAL. This work was funded by the Deutsche Forschungsgemeinschaft (DFG) within the research project “Machining of high-performance materials with ultrasonically modulated cutting speed” (Project number 406283248).

Open Access This article is licensed under a Creative Commons Attribution 4.0 International License, which permits use, sharing, adaptation, distribution and reproduction in any medium or format, as long as you give appropriate credit to the original author(s) and the source, provide a link to the Creative Commons licence, and indicate if changes were made. The images or other third party material in this article are included in the article’s Creative Commons licence, unless indicated otherwise in a credit line to the material. If material is not included in the article’s Creative Commons licence and your intended use is not permitted by statutory regulation or exceeds the permitted use, you will need to obtain permission directly from the copyright holder. To view a copy of this licence, visit <http://creativecommons.org/licenses/by/4.0/>.

References

1. Abootorabi Zarchi MM, Razfar MR, Abdullah A (2017) Research on the importance of tool–workpiece separation in ultrasonic vibration–assisted milling. *Proc Institut Mech Eng Part B: J Eng Manuf* 231(4):600–607. <https://doi.org/10.1177/0954405415581298>
2. Balamuth L (1966) Ultrasonic assistance to conventional metal removal. *Ultrasonics* 4:125–130
3. Cakir FH, Gurgen S, Sofuoğlu MA, Celik ON, Kushan MC (2015) Finite element modeling of ultrasonic assisted turning of Ti6Al4V alloy. *Procedia - Soc Behav Sci* 195:2839–2848. <https://doi.org/10.1016/j.sbspro.2015.06.404>
4. Chen W, Huo D, Shi Y, Hale JM (2018) State-of-the-art review on vibration-assisted milling: principle, system design, and application. *Int J Adv Manuf Technol* 97(5–8):2033–2049. <https://doi.org/10.1007/s00170-018-2073-z>
5. Feng Y, Hsu FC, Lu YT, Lin YF, Lin CT, Lin CF, Lu YC, Liang SY (2019) Residual stress prediction in ultrasonic vibration–assisted milling. *Int J Adv Manuf Technol* 97(5–8):2033. <https://doi.org/10.1007/s00170-019-04109-y>
6. Gillespie LK (1999) *Deburring and edge finishing handbook*. Society of Manufacturing Engineers and American Society of Mechanical Engineers, Dearborn, Mich. and Fairfield
7. Hafiz MSA, Kawaz MHA, Mohamad WNF, Kasim MS, Izamshah R, Saedon JB, Mohamed SB (2017) A review on feasibility study of ultrasonic assisted machining on aircraft component manufacturing. *IOP Conf Series: Mater Sci Eng* 270(012):034. <https://doi.org/10.1088/1757-899X/270/1/012034>
8. Helmecke TP (2018) *Ressourceneffiziente Zerspanung von Ti-6Al-4V-Strukturbauteilen für Luftfahrtanwendungen: Dissertation*. Berichte aus dem IFW 2018:14
9. Maurotto A, Wickramarachchi CT (2016) Experimental investigations on effects of frequency in ultrasonically-assisted end-milling of AISI 316L: a feasibility study. *Ultrasonics* 65:113–120. <https://doi.org/10.1016/j.ultras.2015.10.012>
10. Moriwaki T, Shamoto E (1991) Ultraprecision diamond turning of stainless steel by applying ultrasonic vibration. *CIRP Ann* 40(1):559–562. [https://doi.org/10.1016/S0007-8506\(07\)62053-8](https://doi.org/10.1016/S0007-8506(07)62053-8)
11. Nath C, Rahman M (2008) Effect of machining parameters in ultrasonic vibration cutting. *Int J Mach Tools Manuf* 48(9):965–974. <https://doi.org/10.1016/j.ijmactools.2008.01.013>
12. Nestler A, Schubert A (2014) Surface properties in ultrasonic vibration assisted turning of particle reinforced aluminium matrix composites. *Procedia CIRP* 13:125–130. <https://doi.org/10.1016/j.procir.2014.04.022>
13. Ni C, Zhu L, Liu C, Yang Z (2018) Analytical modeling of tool-workpiece contact rate and experimental study in ultrasonic vibration-assisted milling of Ti–6Al–4V. *Int J Mech Sci* 142–143:97–111. <https://doi.org/10.1016/j.ijmecsci.2018.04.037>
14. Niknam SA, Songmene V (2015) Milling burr formation, modeling and control: a review. *Proc Institut Mech Eng Part B: J Eng Manuf* 229(6):893–909. <https://doi.org/10.1177/0954405414534827>
15. Niu Y, Jiao F, Zhao B, Wang D (2017) Multiobjective optimization of processing parameters in longitudinal-torsion ultrasonic assisted milling of Ti–6Al–4V. *Int J Adv Manuf Technol* 93(9–12):4345–4356. <https://doi.org/10.1007/s00170-017-0871-3>
16. Patil S, Joshi S, Tewari A, Joshi SS (2014) Modelling and simulation of effect of ultrasonic vibrations on machining of Ti6Al4V. *Ultrasonics* 54(2):694–705. <https://doi.org/10.1016/j.ultras.2013.09.010>
17. Razfar MR, Sarvi P, Zarchi MMA (2011) Experimental investigation of the surface roughness in ultrasonic-assisted milling. *Proc Institut Mech Eng Part B: J Eng Manuf* 225(9):1615–1620. <https://doi.org/10.1177/0954405411399331>
18. Rotella G, Dillon OW, Umbrello D, Settineri L, Jawahir IS (2014) The effects of cooling conditions on surface integrity in machining of Ti6Al4V alloy. *Int J Adv Manuf Technol* 71(1–4):47–55. <https://doi.org/10.1007/s00170-013-5477-9>
19. Shamoto E, Suzuki N, Tsuchiya E, Hori Y, Inagaki H, Yoshino K (2005) Development of 3 dof ultrasonic vibration tool for elliptical vibration cutting of sculptured surfaces. *CIRP Ann* 54(1):321–324. [https://doi.org/10.1016/S0007-8506\(07\)60113-9](https://doi.org/10.1016/S0007-8506(07)60113-9)
20. Sharma V, Pandey PM (2016) Recent advances in ultrasonic assisted turning: a step towards sustainability. *Cogent Eng* 3(1):318. <https://doi.org/10.1080/23311916.2016.1222776>
21. Shimada K, Hirai T, Mizutani M, Kuriyagawa T (2019) Unidirectional wetting surfaces fabricated by ultrasonic-assisted cutting. *Int J Autom Technol* 13(2):191–198. <https://doi.org/10.20965/ijat.2019.p0191>
22. Sofuoğlu MA, Çakır FH, Gürgeç S, Orak S, Kuşhan MC (2018) Numerical investigation of hot ultrasonic assisted turning of aviation alloys. *J Brazil Soc Mech Sci Eng* 40(3):391. <https://doi.org/10.1007/s40430-018-1037-4>
23. Thepsonthi T, Özel T (2012) Multi-objective process optimization for micro-end milling of Ti–6Al–4V titanium alloy. *Int J Adv Manuf Technol* 63(9–12):903–914. <https://doi.org/10.1007/s00170-012-3980-z>
24. Tong J, Wei G, Zhao L, Wang X, Ma J (2019) Surface microstructure of titanium alloy thin-walled parts at ultrasonic vibration-assisted milling. *Int J Adv Manuf Technol* 101(1–4):1007–1021. <https://doi.org/10.1007/s00170-018-3005-7>
25. Verma GC, Pandey PM (2019) Machining forces in ultrasonic-vibration assisted end milling. *Ultrasonics* 94:350–363. <https://doi.org/10.1016/j.ultras.2018.07.004>
26. Verma GC, Pandey PM, Dixit US (2018) Estimation of workpiece-temperature during ultrasonic-vibration assisted milling considering acoustic softening. *Int J Mech Sci* 140:547–556. <https://doi.org/10.1016/j.ijmecsci.2018.03.034>

27. Verma GC, Pandey PM, Dixit US (2018) Modeling of static machining force in axial ultrasonic-vibration assisted milling considering acoustic softening. *Int J Mech Sci* 136:1–16. <https://doi.org/10.1016/j.ijmecsci.2017.11.048>
28. Wu C, Chen S, Xiao C, Cheng K, Ding H (2019) Longitudinal-torsional ultrasonic vibration-assisted side milling process. *Proc Institut Mech Eng Part C: J Mech Eng Sci* 233(10):3356–3363. <https://doi.org/10.1177/0954406218819023>
29. Xiangyu Z, Zhenghui L, He S, Deyuan Z (2018) Surface quality and residual stress study of high-speed ultrasonic vibration turning Ti-6Al-4V alloys. *Procedia CIRP* 71:79–82. <https://doi.org/10.1016/j.procir.2018.05.075>
30. Xu WX, Zhang LC (2015) Ultrasonic vibration-assisted machining: principle, design and application. *Adv Manuf* 3(3):173–192. <https://doi.org/10.1007/s40436-015-0115-4>
31. Zhang Y, Zhao B, Wang Y, Chen F (2017) Effect of machining parameters on the stability of separated and unseparated ultrasonic vibration of feed direction assisted milling. *J Mech Sci Technol* 31(2):851–858. <https://doi.org/10.1007/s12206-017-0137-x>
32. Zheng L, Chen W, Huo D (2018) Experimental investigation on burr formation in vibration-assisted micro-milling of Ti-6Al-4V. *Proc Institut Mech Eng Part C: J Mech Eng Sci* 60(095440621879):236. <https://doi.org/10.1177/0954406218792360>
33. Zou Y, Chen G, Lu L, Qin X, Ren C (2019) Kinematic view of cutting mechanism in hole-making process of longitude-torsional ultrasonic assisted helical milling. *Int J Adv Manuf Technol* 103(1–4):267–280. <https://doi.org/10.1007/s00170-019-03483-x>

Publisher's note Springer Nature remains neutral with regard to jurisdictional claims in published maps and institutional affiliations.